

Breaking of brightness consistency in optical flow with a lightweight CNN network

Yicheng Lin¹, Shuo Wang¹, Yunlong Jiang and Bin Han, *Member, IEEE*

Abstract—The sparse optical flow method is a fundamental task in computer vision. However, its reliance on the assumption of constant environmental brightness constrains its applicability in high dynamic range (HDR) scenes. In this study, we propose a novel approach aimed at transcending image color information by learning a feature map that is robust to illumination changes. This feature map is subsequently structured into a feature pyramid and integrated into sparse Lucas-Kanade (LK) optical flow. By adopting this hybrid optical flow method, we circumvent the limitation imposed by the brightness constant assumption. Specifically, we utilize a lightweight network to extract both the feature map and keypoints from the image. Given the challenge of obtaining reliable keypoints for the shallow network, we employ an additional deep network to support the training process. Both networks are trained using unsupervised methods. The proposed lightweight network achieves a remarkable speed of 190fps on the onboard CPU. To validate our approach, we conduct comparisons of repeatability and matching performance with conventional optical flow methods under dynamic illumination conditions. Furthermore, we demonstrate the effectiveness of our method by integrating it into VINS-Mono, resulting in a significantly reduced translation error of 93% on a public HDR dataset. The code implementation is publicly available at <https://github.com/linyicheng1/LET-NET>.

Index Terms—Sparse Optical flow, keypoint detection, deep learning

I. INTRODUCTION

OPTICAL flow refers to the pixels motion between consecutive frames in an image sequence and optical flow method is an algorithm for estimating pixel motion between consecutive images, which includes sparse optical flow method and dense optical flow method. Sparse optical flow method only estimates the pixel motion distance of keypoints, while dense optical flow method estimates in all positions. Optical flow estimation is a classic problem in computer vision. For instance, VINS-Mono [1] and OV²SLAM [2] utilize sparse optical flow method as a key module in visual Simultaneous Localization and Mapping (vSLAM). The performance of optical flow method in HDR scenes determines their robustness to illumination changes. Therefore, the study of illumination-robust optical flow methods is crucial.

The traditional sparse optical flow methods [3], [4] have historically assumed static environmental illumination, which

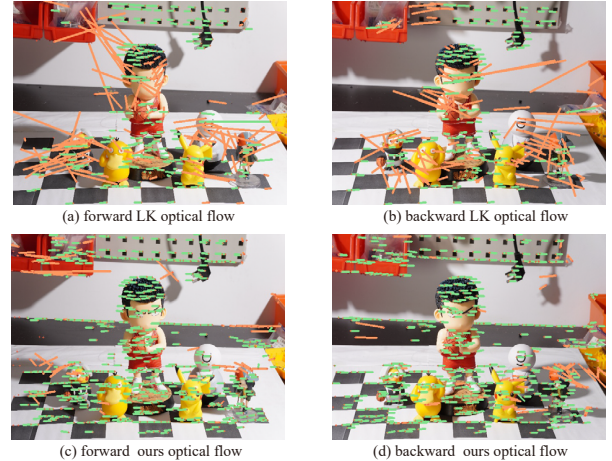


Fig. 1. Examples of dynamic lighting scene images. We collected images under different directions of light to demonstrate the robustness of the proposed method to illumination. Among them, forward optical flow refers to extracting keypoints in the first image and tracking them in the second image. The backward optical flow is the opposite.

limits their effectiveness in HDR scenarios. Although subsequent research [5] have introduced gradient consistency and other higher-order constraints like the constancy of the Hessian and Laplacian to improve illumination robustness, these approaches only partially address this issue. Learning-based dense optical flow methods, such as FlowNet [6], offer a solution to this problem. However, they tend to be less efficient and often require GPU support. Thus, there is no sparse optical flow method capable of real-time execution on CPUs without relying on prior assumptions. Consequently, even the most advanced vSLAM [2] still struggle to maintain robustness in HDR scenes.

We propose a hybrid optical flow method that combines deep learning with traditional approaches to overcome the limitations of conventional methods under HDR scenes. The difference between the hybrid optical flow method and LK optical flow method is clearly demonstrated in Fig. 1. Our approach begins by utilizing a lightweight convolutional neural network (CNN) to extract illumination-invariant feature maps and score maps from images. These feature maps go beyond basic RGB information, encompassing higher-level information. Subsequently, we integrate these feature maps with the traditional pyramid LK optical flow method, as Fig. 2, resulting in the hybrid optical flow method. In our approach, the training process involves two key steps. Firstly, we employ a strategy of assisted training using deep networks to enhance the performance of the lightweight network. Secondly, we introduce new loss functions such as the mask neural

¹These authors contributed equally to this work.

This work was supported in part by the National Natural Science Foundation of China (52375015) and in part by the Natural Science Foundation of Hubei Province of China (2022CFB239). (Corresponding author: Bin Han)

Y. Lin, S. Wang, Y. Jiang and B. Han are with the State Key Laboratory of Intelligent Manufacturing Equipment and Technology, School of Mechanical Science and Engineering, Huazhong University of Science and Technology, Wuhan 430074, China (e-mail: {yichenglin, shuowang99, jiangyunlong binhan}@hust.edu.cn).

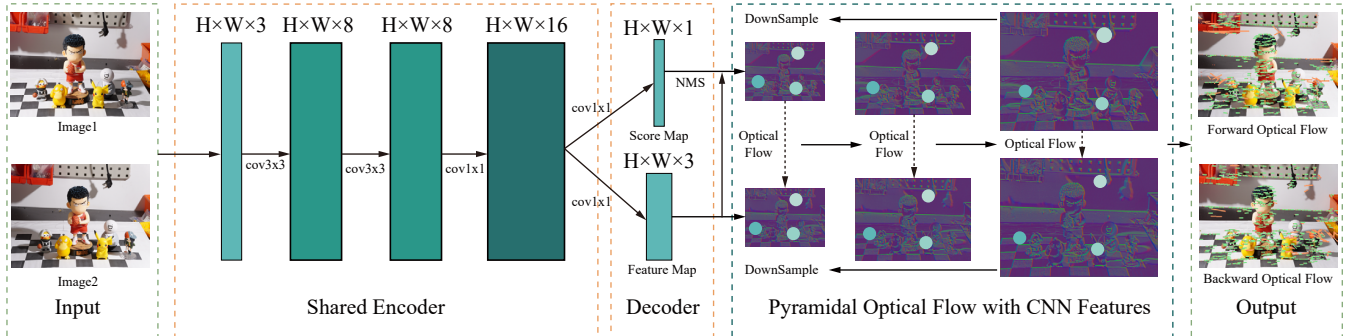


Fig. 2. **The pipeline of the proposed hybrid optical flow method.** A shared encoder is first used to extract the shared feature map of the image, and then the shared feature map are decoded into score map S and illumination-invariant feature map F . The score map S is utilized for extracting keypoints, employing non-maximum suppression (NMS) to identify them. The illumination-invariant feature map F are used to construct the pyramid optical flow method. Following the pyramid LK optical flow method, the hybrid optical flow method begins tracking the extracted keypoints from the highest level of the feature pyramid. The feature map are utilized to locate the positions of these keypoints in another image. Subsequently, the tracking results from the upper level are utilized as initial values for the tracking computation in the lower level, ultimately yielding sparse optical flow results.

reprojection error (mNRE) loss to learn illumination-invariant features and the line peaky loss learn keypoint scores. The hybrid optical flow method achieves both efficient and accurate optical flow computation while demonstrating robustness to changes in illumination. In summary, the main contributions of this paper are as follows:

- 1) We propose a hybrid optical flow method that does not rely on brightness consistency assumptions and can work properly in HDR environments.
- 2) We propose a loss function mNRE for extracting light invariants in images, and improve the peaky loss in keypoint extraction.
- 3) We propose to use a deep network to train and a shallow network to infer, balancing performance and efficiency, reaching 190Hz on the CPU.

II. RELATED WORK

A. Traditional optical flow method

Horn and Schunck (HS) [7] proposed the first truly optical flow method, which formulated optical flow estimation as an optimisation problem minimising the global energy function. Gaussian filtering has been introduced as a pre-processing operation in variational methods to improve the performance in noisy conditions [8]. In contrast to HS, which computes the optical flow field for the entire image, Lucas et al. [3] proposed a method to track the optical flow for specific points. To address the issue of insufficient pixel displacement in real scenes, Bouguet [9] proposed a pyramid structure to implement the coarse-to-fine pyramidal Lucas Kanade (PLK). To improve the robustness of illumination, [5] proposed gradient consistency and other higher-order consistency constraints, such as constancy of the Hessian and constancy of the Laplacian. Robust Local Optical Flow (RLOF) [10], [11] proposes the adjustment of the neighbourhood window size to solve the generalised aperture problem. While employing these methods can enhance the robustness of optical flow, they are unable to fundamentally resolve the issue.

B. Learning-based optical flow method

CNN were first used to compute optical flow by Dosovitskiy [6]. Two end-to-end networks, FlowNetS and FlowNetC, were proposed to learn optical flow directly from the synthetic annotated Flying Chairs dataset. The accuracy of the optical flow estimation has been improved by the addition of sub-networks for small displacements in FlowNet [12]. Inspired by iterative updates, Recurrent All-Pairs Field Transforms (RAFT) [13] proposed a new network architecture for optical flow estimation, and [14] further improved its detection efficiency. Although end-to-end methods are designed to be as lightweight as possible, the complexity of optical flow estimation still limits real-time computation to GPUs.

C. Keypoint detection

Classical Harris [15] keypoint detection uses the autocorrelation matrix to search for keypoints. To enhance the tracking performance of the keypoints, Shi and Tomasi [16] proposed a selection criterion that makes the keypoints more distributed, which has been widely used in optical flow methods. In addition, SIFT [17], ORB [18] etc. geometric methods were proposed to extract keypoints and matched by descriptors.

Inspired by handcrafted feature detectors, a common approach for CNN-based detection is to construct response maps to locate interest points in a supervised manner [19]. SuperPoint [20] subsequently suggested self-supervised learning using a pre-trained model to generate pseudo-ground truth points. Furthermore, unsupervised training methods are used to extract keypoints, KeyNet [21] and others. To overcome the problem of non-differentiable Non-maximum suppression (NMS), ALIKE [22] propose differentiable feature point detection modules.

The proposed method does not belong to either traditional optical flow or end-to-end learning-based optical flow. It combines learning-based approaches with traditional methods, striking a balance between computational efficiency and performance. We refer to it as a hybrid optical flow method.

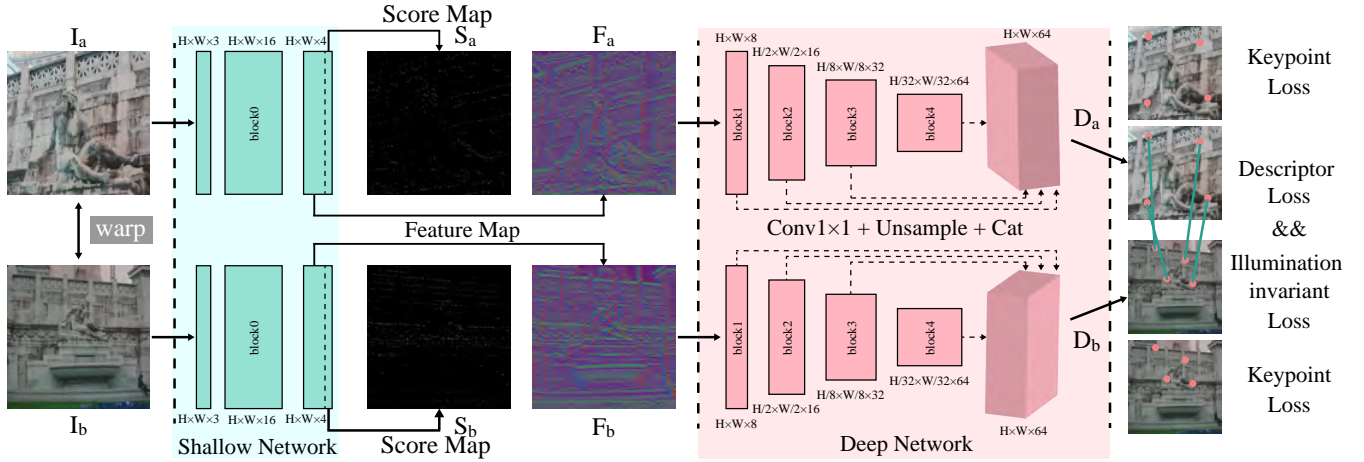


Fig. 3. **The network training process.** A shallow network is first used to extract the score map \mathbf{S} and feature map \mathbf{F} . Then, in order to supervise the reliability of the training keypoints, a deep network is used to extract the dense descriptor map \mathbf{D} . Finally, we calculate the keypoint loss, feature loss and descriptor loss based on the results of $[\mathbf{S}, \mathbf{F}, \mathbf{D}]$. Only the shallow network was used for the hybrid optical flow method depicted in Fig. 2, while the deep network was only used for training.

III. HYBRID OPTICAL FLOW METHOD

A. Network architecture

As illustrated in Fig. 2, the network is designed to be as lightweight as possible which only uses four convolution operations. First, shared feature map of size $W \times H \times 16$ are extracted from the input image ($W \times H \times 3$). The shared feature map is then transformed into an illumination-invariant feature map and a keypoint score map, using a 1×1 convolution kernel. With the lightweight network, the illumination-invariant feature map contains less high-level semantic information while retaining more low-level image information. We consider that the low-level information is sufficient for our tasks. Therefore, the computation complexity of the designed network is much lower than other ones. Each of these is explained in more detail as follows:

- (a) **Shared Encoder** The image feature encoder converts the input image $I \in W \times H \times 3$ to the size $W \times H \times 16$. The first two convolution operations use a 3×3 convolution kernel and expand the shared feature map to 8 channels. In the last layer, a 1×1 convolution kernel is used to increase the number of channels up to 16. The ReLU [23] activation function is used after each convolution. We keep the original image resolution in all convolution operations.
- (b) **Feature and Score Map Decoder** The shared feature map is decoded into a score map and an illumination-invariant feature map by the decoding layer. It uses a 1×1 convolution kernel to reduce the channels of the feature map to 4. The first three channels are the illumination-invariant feature map, and the last channel is the keypoint score map. After the convolution, the score map is activated by the sigmoid function to limit its value between $[0, 1]$. The convolution feature map is also L2 normalised. So we get the final output with a score map of $W \times H \times 1$ and an illumination-invariant feature map of $W \times H \times 3$.

B. Optical flow method with illumination-invariant feature maps

The keypoint is first extracted from the score map. Then, we use it as the initial position of the optical flow method. Based on the LK optical flow method, we modify the brightness consistency assumption to illumination-invariant feature consistency, i.e. the convolution feature vector of the same keypoint position in different images is the same. Assuming that, a new hybrid optical flow method is proposed in combination with the pyramidal optical flow method.

1) *Keypoint extraction:* The optical flow method expects a more uniform distribution of keypoints to improve the overall tracking robustness. So we use a method similar to the *GoodFeaturesToTrack* function in OpenCV to extract keypoints. First, the local maximum in the 3×3 neighbourhood is retained by NMS, and then the keypoints with lower scores than the threshold are removed. We then use the maximum interval sampling method to ensure a uniform distribution of the keypoints.

2) *Pyramid optical flow method:* According to [4], pyramid optical flow method can be divided into three steps. First, the spatial and temporal derivatives of the illumination-invariant feature map $\mathbf{F}(x, y, t)$, namely \mathbf{F}_x , \mathbf{F}_y and \mathbf{F}_t , are computed. Then, the derivatives of all keypoints are combined into a coefficient matrix \mathbf{A} and a constant vector \mathbf{b} , respectively given by

$$\mathbf{A} = \begin{bmatrix} [\mathbf{F}_x & \mathbf{F}_y]_1 \\ \vdots \\ [\mathbf{F}_x & \mathbf{F}_y]_k \end{bmatrix}, \mathbf{b} = \begin{bmatrix} -\mathbf{F}_{t1} \\ \vdots \\ -\mathbf{F}_{tk} \end{bmatrix}, \quad (1)$$

where k is the number of keypoints. Finally, the optical flow velocity \mathbf{v} is obtained by solving the equation $\mathbf{A}\mathbf{v} = \mathbf{b}$. In our method, we use the standard LK optical flow algorithm, but modify the brightness constancy assumption to a convolution feature constancy assumption. Therefore, our method is called the hybrid optical flow method.

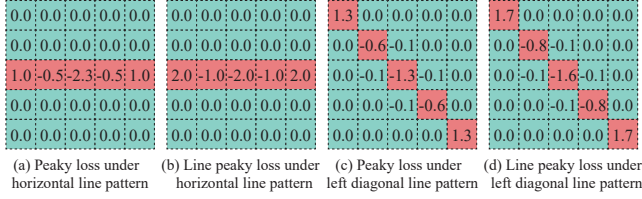


Fig. 4. **Comparison of line peaky loss and peaky loss.** In 5×5 sized patch, the cyan block represents score 0.5 while the red represents score 1. The numbers in the blocks represent then the derivative of the different losses with respect to the block. It can be seen that the line peaky loss increases the penalty weight for the ends of the lines.

IV. LEARNING TRACKED KEYPOINTS AND INVARIANT FEATURE

Fig. 3 illustrates the training process of the network. For an image pair, a shallow network is used for the extraction of the score map \mathbf{S} and the feature map \mathbf{F} , and a deep network is used for the extraction of the dense descriptor map \mathbf{D} . The shallow network here is consistent with the network structure in Sec. III while the deep network is only used to assist in training. The keypoint loss, the illumination invariant feature loss, and the descriptor loss are used to train the three distinct outputs $[\mathbf{S}, \mathbf{F}, \mathbf{D}]$, respectively. The keypoint loss consists of reprojection loss, line peaky loss and reliability loss. The NRE function and the proposed mNRE function are used for descriptor loss and illumination invariant feature loss, respectively.

A. Keypoint loss

As described in previous work [22], a good keypoint should be repeatable, highly accurate, and matchable. Thus, three loss functions are used to train for the extraction of keypoints. The reprojection loss function ensures the repeatability of the keypoints. The line peaky loss function is beneficial for accuracy improvement of keypoints. And loss of reliability makes it easier to match the extracted keypoints.

1) *Reprojection loss*: A keypoint should be extracted simultaneously in two images under different conditions. The reprojection error is defined as the distance between the projected point and the extracted point. A point \mathbf{p}_A in image \mathbf{I}_A is projected to image \mathbf{I}_B , and the projection point is \mathbf{p}_{AB} . The single reprojection error is

$$\text{dist}_{AB} = \|\mathbf{p}_{AB} - \mathbf{p}_B\|, \quad (2)$$

where \mathbf{p}_B is the extracted point in image \mathbf{I}_B and $\|\cdot\|$ is 2-norm of the vector. The reprojection error loss is defined in a symmetrical form

$$\mathcal{L}_{rp} = \frac{\sum_{i=0}^{N-1} \text{dist}_{AB}^i}{N} + \frac{\sum_{i=0}^{M-1} \text{dist}_{BA}^i}{M}, \quad (3)$$

where N is the number of points in image \mathbf{I}_A that can be found in image \mathbf{I}_B , dist_{AB}^i is the reprojection error of the i th feature out of the N features, M is the number of points in image \mathbf{I}_B that can be found in image \mathbf{I}_A , and dist_{BA}^i is the reprojection error of the i th feature out of the M features.

2) *Line peaky loss*: On the score map, keypoints should take on a peaked shape in the neighborhood. Consider a $N \times N$ -sized patch near the keypoint \mathbf{p} on the score map, the distance between each pixel location $[i, j]$ and the keypoint is

$$d(\mathbf{p}, i, j) = \{\|\mathbf{p} - [i, j]\|\}, \quad (4)$$

where $\|\cdot\|$ is a 2-norm of the vector. The peaky loss proposed by [22] is used to reduce the score of farther-distant positions within a patch, defined as

$$\mathcal{L}_{pk}(\mathbf{p}) = \frac{1}{N^2} \sum_{0 \leq i, j < N} d(\mathbf{p}, i, j) s(\mathbf{p}, i, j), \quad (5)$$

where $s(\mathbf{p}, i, j)$ is the score corresponding to the position $[i, j]$ in the patch near the keypoint \mathbf{p} . This definition views all pixels within the patch uniformly, making the score map form a locally linear shape during training. Thus, we consider four line patterns, horizontal, vertical, left diagonal, and right diagonal, with increased penalty weights for line shapes. In a patch of size $N \times N$ near the keypoint \mathbf{p} , the four line weights w_1, w_2, w_3, w_4 are defined as

$$\begin{aligned} w_1(\mathbf{p}, i, j) &= \mathcal{N}(|i - p_x|) \\ w_2(\mathbf{p}, i, j) &= \mathcal{N}(|j - p_y|) \\ w_3(\mathbf{p}, i, j) &= \mathcal{N}(|i + j - p_x - p_y|) \\ w_4(\mathbf{p}, i, j) &= \mathcal{N}(|i - j - p_x + p_y|) \end{aligned} \quad (6)$$

where $[i, j]$ is the pixel position within the patch, p_x, p_y are the coordinates of the keypoint \mathbf{p} , \mathcal{N} is the gaussian distribution and $|\cdot|$ is the 1-norm. By using these weights, the line peaky loss are defined as

$$\begin{aligned} s(\mathbf{p}, i, j) &= w_k(\mathbf{p}, i, j) d(\mathbf{p}, i, j) s(\mathbf{p}, i, j) \\ \mathcal{L}_{lpk}(\mathbf{p}) &= \max_{k=1 \dots 4} \left\{ \frac{1}{N^2} \sum_{[i, j]^T \in \text{patch}(\mathbf{p})} s(\mathbf{p}, i, j) \right\}, \end{aligned} \quad (7)$$

where the max function is used to select the maximum value from the four line patterns. Fig. 4 demonstrates that the peaky loss differs from the derivative of the proposed line peaky loss in that the penalty at the ends of the line is increased by the line peaky loss.

3) *Reliability loss*: Accurate and repeatable keypoints are not sufficient. It is also necessary to ensure the matchability of the keypoints [22]. To compute the matchability of the keypoint \mathbf{p}_A in image \mathbf{I}_A , the vector distance between its corresponding descriptor $\mathbf{d}_{\mathbf{p}_A} \in \mathbb{R}^{dim}$ and the dense descriptor map $\mathbf{D}_B \in \mathbb{R}^{H \times W \times dim}$ in image \mathbf{I}_B are computed as

$$\mathbf{C}_{\mathbf{d}_{\mathbf{p}_A}, \mathbf{D}_B} = \mathbf{D}_B \mathbf{d}_{\mathbf{p}_A}, \quad (8)$$

where $\mathbf{C}_{\mathbf{d}_{\mathbf{p}_A}, \mathbf{D}_B} \in \mathbb{R}^{H \times W}$ is known as the similarity map representing the similarity between the keypoint \mathbf{p}_A and the position of each pixel in the image \mathbf{I}_B . The normalization function then makes the score of the positions with high similarity to 1, while the score of the positions with low similarity is 0, thus the matching probability map $\tilde{\mathbf{C}}_{\mathbf{d}_{\mathbf{p}_A}, \mathbf{D}_B} \in \mathbb{R}^{H \times W}$ is defined as

$$\tilde{\mathbf{C}}_{\mathbf{d}_{\mathbf{p}_A}, \mathbf{D}_B} = \exp\left(\frac{\mathbf{C}_{\mathbf{d}_{\mathbf{p}_A}, \mathbf{D}_B} - 1}{t}\right), \quad (9)$$

where \exp is the exponential function used to compose the normalization function, and $t = 0.02$ controls the shape of the function. For the keypoint \mathbf{p}_A , the higher matching probability of its projected location \mathbf{p}_{AB} implies its higher reliability. Therefore the reliability $r_{\mathbf{p}_A}$ of the keypoint \mathbf{p}_A is defined as

$$r_{\mathbf{p}_A} = \mathbf{bisampling}(\tilde{\mathbf{C}}_{\mathbf{d}_{\mathbf{p}_A}, \mathbf{D}_B}, \mathbf{p}_{AB}), \quad (10)$$

where $\mathbf{bisampling}(\mathbf{M}, \mathbf{p})$ is a function of bilinear sampling of the $\mathbf{M} \in \mathbb{R}^{H \times W}$ at position $\mathbf{p} \in \mathbb{R}^2$. Then consider all the keypoints in the image \mathbf{I}_A and penalize the keypoint scores that are less reliable among them to get the reliability loss

$$\begin{aligned} \mathbb{S} &= \sum_{\substack{\mathbf{p}_A \in \mathbf{I}_A \\ \mathbf{p}_{AB} \in \mathbf{I}_B}} s_{\mathbf{p}_A} s_{\mathbf{p}_{AB}} \\ \mathcal{L}_{reliability}^A &= \frac{1}{N_A} \sum_{\substack{\mathbf{p}_A \in \mathbf{I}_A \\ \mathbf{p}_{AB} \in \mathbf{I}_B}} \frac{s_{\mathbf{p}_A} s_{\mathbf{p}_{AB}}}{\mathbb{S}} (1 - r_{\mathbf{p}_A}), \end{aligned} \quad (11)$$

where N_A is the number of all keypoints in the image \mathbf{I}_A , $s_{\mathbf{p}_A}$ is the score of the keypoint \mathbf{p}_A and $s_{\mathbf{p}_{AB}}$ is the score of the projection location.

Based on the above three loss functions, we obtain the keypoint loss

$$\begin{aligned} \mathcal{L}_{keypoint} &= k_1 \cdot \mathcal{L}_{rp} + \\ &k_2 \cdot \frac{1}{N + M} \left(\sum_{\mathbf{p}_A \in \mathbf{I}_A} \mathcal{L}_{lpk}(\mathbf{p}_A) + \sum_{\mathbf{p}_B \in \mathbf{I}_B} \mathcal{L}_{lpk}(\mathbf{p}_B) \right) + \\ &k_3 \cdot \frac{1}{2} (\mathcal{L}_{reliability}^A + \mathcal{L}_{reliability}^B) \end{aligned} \quad (12)$$

where $k_1 = 1, k_2 = 0.5, k_3 = 1$ are the weights and N, M are the number of keypoints in image \mathbf{I}_A and \mathbf{I}_B respectively.

B. Descriptor loss

The NRE [24] function was used to learn the descriptors. Due to its good performance, we adopted it as the descriptor loss. Previous work [22] explains the derivation and definition of NRE function by the cross-entropy function. We give an explanation from another more intuitive perspective. Based on the similarity map defined in Eq. 8, a new matching probability map $\tilde{\mathbf{C}}_{\mathbf{d}_{\mathbf{p}_A}, \mathbf{D}_B} \in \mathbb{R}^{H \times W}$ is defined as

$$\tilde{\mathbf{C}}_{\mathbf{d}_{\mathbf{p}_A}, \mathbf{D}_B} := \mathbf{softmax} \left(\frac{C_{\mathbf{d}_{\mathbf{p}_A}, \mathbf{D}_B} - 1}{t} \right), \quad (13)$$

where the normalization function $\mathbf{softmax}$ converts similarity to probability and satisfies that all elements sum to one, i.e., $\sum_{H \times W} \tilde{\mathbf{C}}_{\mathbf{d}_{\mathbf{p}_A}, \mathbf{D}_B} = 1$. For a good descriptor $\mathbf{d}_{\mathbf{p}_A}$, it should be as similar as possible to the descriptor at projection position \mathbf{p}_{AB} and far away from all other descriptors. Thus, by the same sampling function in Eq. 10, we get the matching probability $p_{\mathbf{d}_{\mathbf{p}_A}, \mathbf{D}_B}^{\mathbf{p}_{AB}}$ as

$$p_{\mathbf{d}_{\mathbf{p}_A}, \mathbf{D}_B}^{\mathbf{p}_{AB}} = \mathbf{bisampling}(\tilde{\mathbf{C}}_{\mathbf{d}_{\mathbf{p}_A}, \mathbf{D}_B}, \mathbf{p}_{AB}). \quad (14)$$

Maximizing the matching probability at the projected positions $p_{\mathbf{d}_{\mathbf{p}_A}, \mathbf{D}_B}^{\mathbf{p}_{AB}}$ with the constraint that the sum of all the elements is equal to 1 implies minimizing the matching probability at the

other positions. The descriptor loss function is then obtained as

$$\mathcal{L}_{desc} = \frac{1}{N_A + N_B} \cdot \left(- \sum_{\mathbf{p}_A \in \mathbf{I}_A} \ln(p_{\mathbf{d}_{\mathbf{p}_A}, \mathbf{D}_B}^{\mathbf{p}_{AB}}) - \sum_{\mathbf{p}_B \in \mathbf{I}_B} \ln(p_{\mathbf{d}_{\mathbf{p}_B}, \mathbf{D}_A}^{\mathbf{p}_{BA}}) \right), \quad (15)$$

where N_A is the number of keypoints in image \mathbf{I}_A , N_B is the number of keypoints in image \mathbf{I}_B , and the $-\ln(\cdot)$ function converts the maximization problem into a minimization problem.

C. Illumination-invariant feature loss

The illumination invariant feature map is similar to the dense descriptor map in that both attempt to extract features in an image that do not vary with viewing point and illumination. The difference is that descriptors are usually obtained using 64 or 128 channels and are convolved several times, whereas illumination invariant feature maps have only three or one channel and are obtained by four convolutions. Thus illumination invariant feature maps are difficult to learn to obtain features that are distinguishable over the entire image. Therefore we propose to learn locally distinguishable illumination invariant feature maps using mNRE loss function. Consider first defining the mask function near the keypoint $\mathbf{p} = [p_x, p_y]^T$

$$\text{mask}(\mathbf{p}) = \begin{cases} 1 & \text{if } \max(|x - p_x|, |y - p_y|) < d \\ 0 & \text{otherwise} \end{cases}, \quad (16)$$

where $d = 80$ is the mask range and $|\cdot|$ is the 1-norm. This mask is then added to Eq. 13 of the NRE loss function to obtain the local matching probability map

$$m_{\tilde{\mathbf{C}}_{\mathbf{d}_{\mathbf{p}_A}, \mathbf{D}_B}} := \mathbf{softmax} \left(\frac{\text{mask}(\mathbf{p}_A) \cdot C_{\mathbf{d}_{\mathbf{p}_A}, \mathbf{D}_B} - 1}{t} \right), \quad (17)$$

where $m_{\tilde{\mathbf{C}}_{\mathbf{d}_{\mathbf{p}_A}, \mathbf{D}_B}} \in \mathbb{R}^{H \times W}$ has a value of zero in the region away from \mathbf{p}_A . Then similar to in the NRE loss, we computed the local matching probability of the projected positions

$$m_{\mathbf{d}_{\mathbf{p}_A}, \mathbf{D}_B}^{\mathbf{p}_{AB}} = \mathbf{bisampling} \left(m_{\tilde{\mathbf{C}}_{\mathbf{d}_{\mathbf{p}_A}, \mathbf{D}_B}}, \mathbf{p}_{AB} \right). \quad (18)$$

Finally, the loss function is computed based on the local matching probability of all keypoints in images \mathbf{I}_A and \mathbf{I}_B as

$$\mathcal{L}_{feat} = \frac{1}{N_A + N_B} \cdot \left(- \sum_{\mathbf{p}_A \in \mathbf{I}_A} \ln(m_{\mathbf{d}_{\mathbf{p}_A}, \mathbf{D}_B}^{\mathbf{p}_{AB}}) - \sum_{\mathbf{p}_B \in \mathbf{I}_B} \ln(m_{\mathbf{d}_{\mathbf{p}_B}, \mathbf{D}_A}^{\mathbf{p}_{BA}}) \right). \quad (19)$$

V. EXPERIMENTS

A. Training Details

MegaDepth [25] is used to train the model. All images in the dataset are scaled to 480×480 during the training process. Training is done using the ADAM [26] optimiser with a learning rate of $3e^{-3}$. We set the batch size to one, but use the gradient of 16 batches to accumulate, and train for 100 epochs. Using the above settings, our model was trained on a 4090 graphics card for approximately one day.

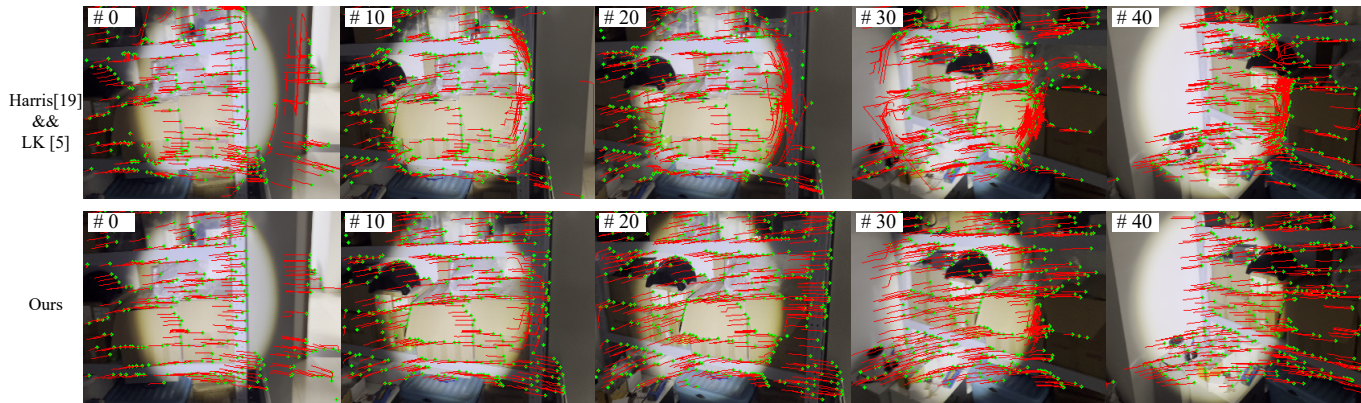


Fig. 5. **Optical flow method comparison in image sequences.** In the image sequence, an active light source is used to simulate dynamic lighting environments. At the edge of the elliptical spot, the constant brightness assumption no longer holds, so the performance of the optical flow method will be challenged. The current keypoints are drawn in green, and the optical flow results within ten frames is drawn in red. Image pairs in the sequence are drawn every ten frames. It can be seen that the traditional LK optical flow method has a large error at the edge of the spot. The proposed optical flow method has significantly improved performance at the edge of the spot.

TABLE I
REPEATABILITY COMPARISON

Method	Repeatability \uparrow		CPU time(ms) \downarrow
	Illumination Scenes	Viewpoint Scenes	
Ours	0.618	0.606	5.2
ALike(T) [22]	0.638	0.563	84.4
SuperPoint [20]	0.652	0.503	93.5
Harris [15]	0.62	0.556	4.9
Fast [27]	0.575	0.552	0.4
Random	0.101	0.1	/

B. HPatches Repeatability

In order to verify the performance of the proposed model in the detection of keypoints, we calculated the repeatability of the keypoints on the HPatches [28] dataset. We compared the proposed method with ALIKE(T) [22], SuperPoint [20], Harris [15], Fast [27], Random. The repeatability is calculated for the extraction of 300 keypoints at a resolution of 240×320 . The same NMS is used for all feature point detection methods to suppress the phenomenon of feature point clustering. The keypoints with reprojection distance less than 3 in the two images are considered to be repeat keypoints and the keypoints above this threshold are not repeatable. The comparison of repeatability in illumination scenes and viewpoint scenes is shown in the table I. We can see that the proposed keypoint point repetition rate is at the state-of-the-art level.

In terms of calculation time, all methods are run on the same onboard CPU I7-1165G7 and measured. We computed the non-deep learning keypoint extraction method in the size of 480×640 , and computed the deep learning keypoint score map in 240×320 , and then upsampled to 480×640 . From the table I, it can be seen that the proposed method has greatly improved the real-time performance compared to other deep learning solutions, and even comparable to traditional methods.



(a) Indoor (b) Light Source (c) Outdoor (d) Image Blur

Fig. 6. **Examples of dynamic lighting scene images.** The collected data contains four typical scenes, indoor light source changes, active light sources, outdoor sunlight changes and image blur caused by light scattering. The gray scale assumption is not satisfied in all image pairs.

TABLE II
CORRECT TRACKING RATIO

Scenes	Indoor	Lighting Source	Outdoor	Image Blur
Ours	0.84	0.87	0.67	0.75
LK Optical Flow [4]	0.58	0.37	0.45	0.19
Census	0.53	0.72	0.61	0.41
Histogram equalization	0.51	0.50	0.52	0.49
ORB [18]	0.12	0.40	0.23	0.32
ALIKE(T) [22]	0.59	0.41	0.54	0.51
SuperPoint [20]	0.48	0.49	0.57	0.51

C. Keypoint Tracking

We collected several sets of image pairs with typical lighting changes and active light sequences. Fig. 6 shows some examples of collected images. These scenes are divided into four typical categories, namely indoor light source changes, outdoor sunlight changes, active light sources and image blur.

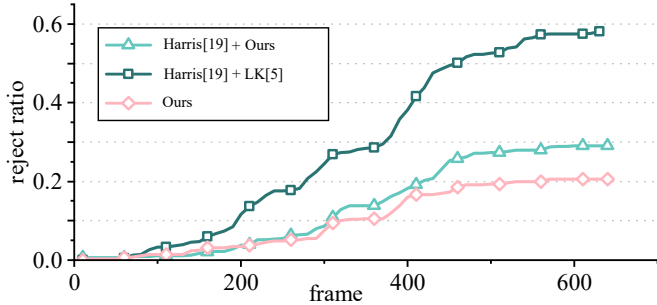


Fig. 7. **Keypoint tracking rejection rate.** In the sequence with active light source, the number of outliers in the optical flow matching is counted and divided by the total number of keypoints to obtain the rejection rate. Compared with the original LK optical flow method, the proposed method can effectively reduce the number of outliers, thereby improving the accuracy of optical flow.

Each category collects five pairs of images with small angle differences but large illumination changes.

Using the data, we compared the proposed methods’ matching results in Table II. All methods run on images sized 480×640 and restrict to extracting up to 300 keypoints for matching. Brute force matching is used to obtain matching results for all keypoints with descriptors such as ORB [18]. The optical flow method after preprocessing the image using census transform and histogram equalization was similarly compared. As there is no ground truth, we match each set of frames using SIFT [17] keypoints and estimate the fundamental matrix in RANSAC [29]. This matrix serves to filter all matches to obtain the correct number. Table II shows the comparison of the correct tracking rate in different scenes. From the table, we can see that the proposed method has achieved the highest correct tracking rate in all scenes.

For further verification of the performance of the proposed method in dynamic lighting scenes, we also collected a sequence with an active light source. As in the VIO system, we continuously tracked the positions of the extracted keypoints in the sequence. As shown in Fig. 5, the proposed method can continuously track keypoints at the edge of the spot. Furthermore, Fig. 7 shows that the proposed method can continuously track keypoints in scenes with illumination changes. The traditional optical flow method fails due to the interference of the active light source, resulting in a rapid increase in the rejection rate.

D. VIO Trajectory Estimation

We embed the proposed optical flow method into the modern VIO system, VINS-Mono [1]. By replacing the original keypoint extraction algorithm and the optical flow method calculation method, the modified VIO system is obtained. As shown in Fig. 8, a comparison test was performed on the UMA-VI [30] dataset with dynamic lighting data. As the dataset only provides the part of the ground truth, we only compute the final trajectory translation error, as shown in table III. We similarly tested this in the widely used EuRoC [31] dataset, as in table IV. The results show that hybrid optical flow can equally improve the accuracy even in common datasets.

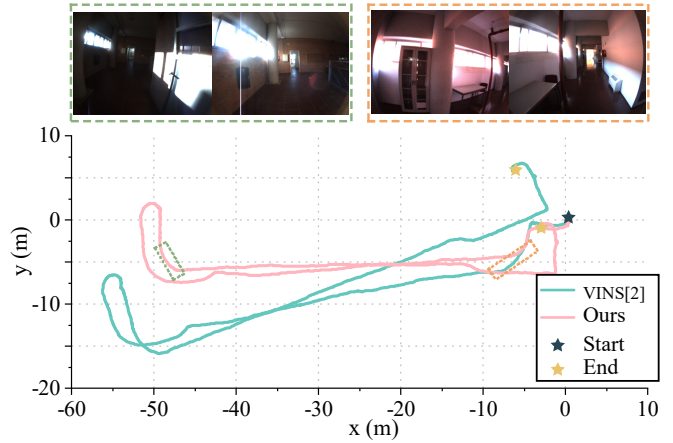


Fig. 8. **Sequence 1 trajectory comparison in the UMA-VI [30] dataset.** The starting point and end point of the sequence coincide, and it can be seen that the improved method can effectively improve the accuracy of the trajectory in the dynamic lighting scene. The two set of pictures corresponding to the two parts of the rapid accumulation of trajectory error are displayed above the curve, which verifies that the rapid change of lighting is the main source of error.

TABLE III
TRAJECTORY ERROR COMPARISON IN INDOOR-OUTDOOR DYNAMIC ILLUMINATION CATEGORY

Trajectory Error ↓	VINS [1]	VINS(Ours)	ORB-SLAM3 [32]
two-floors-csc1	8.97	2.96	lost
two-floors-csc2	17.81	10.67	lost

TABLE IV
COMPARISON OF TRAJECTORY ERRORS ON THE EUROC DATASET

Sequence	Method	APE_{rot}	APE_{trans}	RPE_{rot}	RPE_{trans}
V1_02	Ours	3.65	0.16	0.18	5.0e-2
	VINS	3.73	0.12	0.22	4.5e-2
V1_03	Ours	2.48	0.08	0.21	5.7e-2
	VINS	5.56	0.15	0.25	6.9e-2
V1_04	Ours	3.36	0.13	0.19	4.0e-2
	VINS	3.65	0.16	0.18	3.9e-2
MH_03	Ours	1.48	0.12	0.10	6.8e-2
	VINS	1.69	0.19	0.11	5.9e-2
MH_04	Ours	1.80	0.15	0.14	6.3e-2
	VINS	1.87	0.18	0.16	6.2e-2

E. Ablation experiment

This subsection contains two comparison experiments that validate the line peaky loss and the mNRE loss, respectively. The keypoint repeatability obtained after training with peak loss and line peak loss is shown in table V. During the repeatability calculations NMS radius was 2 and the number of keypoints was 400 and performed on the original image size. Similarly, the percentage of correct tracking obtained by training the illumination invariant feature maps using mNRE loss and NRE loss, respectively, is shown in table VI. It can be seen that mNRE can effectively improve the quality of optical flow tracking. The experimental parameters are set up in the same way as V-C.

TABLE V
REPEATABILITY IN HPATCHES

Training steps	10	20	30	40	50
peaky	0.20	0.22	0.23	0.22	0.23
line peaky	0.32	0.36	0.37	0.39	0.40

TABLE VI
CORRECT TRACKING RATIO

Scenes	Indoor	Lighting Source	Outdoor	Image Blur
NRE	0.92	0.84	0.68	0.44
mNRE	0.96	0.91	0.71	0.74

VI. CONCLUSIONS

In this paper, we propose a hybrid sparse optical flow method that maintains the real-time performance of traditional optical flow method while improving its robustness in dynamic lighting scenes. The basic idea of this work is that CNN are suitable for extracting image features, while traditional LK optical flow method is suitable for optical flow calculation. The combination of the two methods improves the performance of the optical flow method. To achieve this goal, we propose a lightweight network for extracting keypoints and an illumination-invariant feature map. We also propose a training process assisted by a deep network for the shallow network proposed, and multiple loss functions for training the network. The repeatability of the proposed method is verified on the HPatches dataset, and its performance in dynamic lighting scenes is verified on multiple dynamic lighting datasets. Finally, it is embedded in the VIO system to verify its effectiveness in practical applications. This work will support the development of illumination-robust visual SLAM with the hope of achieving robust performance in challenging environments such as caves and tunnels.

REFERENCES

- [1] T. Qin, P. Li, and S. Shen, "VINS-Mono: A robust and versatile monocular visual-inertial state estimator," *IEEE Trans. Robotics*, vol. 34, no. 4, pp. 1004–1020, 2018.
- [2] M. Ferrera, A. Eudes, J. Moras, M. Sanfourche, and G. Le Besnerais, "OV²SLAM : A fully online and versatile visual SLAM for real-time applications," *IEEE Robot. Autom. Lett. (RA-L)*, 2021.
- [3] B. D. Lucas and T. Kanade, "An iterative image registration technique with an application to stereo vision," in *Int. Joint Conf. Artif. Intell.*, vol. 2, 1981, pp. 674–679.
- [4] J.-Y. Bouguet *et al.*, "Pyramidal Implementation of the affine Lucas Kanade Feature Tracker Description of the Algorithm," *Intel corporation*, vol. 5, no. 1-10, p. 4, 2001.
- [5] N. Papenberger, A. Bruhn, T. Brox, S. Didas, and J. Weickert, "Highly accurate optic flow computation with theoretically justified warping," *Int. J. Comput. Vis.*, vol. 67, pp. 141–158, 2006.
- [6] A. Dosovitskiy, P. Fischer, E. Ilg, P. Hausser, C. Hazirbas, V. Golkov, P. Van Der Smagt, D. Cremers, and T. Brox, "FlowNet: Learning Optical Flow with Convolutional Networks," in *IEEE Int. Conf. Comput. Vis. (ICCV)*, 2015, pp. 2758–2766.
- [7] B. K. Horn and B. G. Schunck, "Determining optical flow," *Artif. Intell.*, vol. 17, no. 1-3, pp. 185–203, 1981.
- [8] H. Zimmer, A. Bruhn, and J. Weickert, "Optic flow in harmony," *Int. J. Comput. Vis.*, vol. 93, pp. 368–388, 2011.
- [9] J.-Y. Bouguet *et al.*, "Pyramidal Implementation of the Lucas Kanade Feature Tracker Description of the algorithm," *Intel corporation*, vol. 5, no. 1-10, p. 4, 2001.

- [10] T. Senst, V. Eiselein, and T. Sikora, "Robust Local Optical Flow for Feature Tracking," *IEEE Trans. Circuits Syst. Video Technol.*, vol. 22, no. 9, pp. 1377–1387, 2012.
- [11] T. Senst, J. Geistert, and T. Sikora, "Robust local optical flow: Long-range motions and varying illuminations," in *IEEE Int. Conf. Image Process.*, 2016, pp. 4478–4482.
- [12] E. Ilg, N. Mayer, T. Saikia, M. Keuper, A. Dosovitskiy, and T. Brox, "FlowNet 2.0: Evolution of Optical Flow Estimation with Deep Networks," in *IEEE Conf. Comput. Vis. Pattern Recognit. (CVPR)*, 2017, pp. 2462–2470.
- [13] Z. Teed and J. Deng, "RAFT: Recurrent All-Pairs Field Transforms for Optical Flow," in *European Conference on Computer Vision*, 2020, pp. 402–419.
- [14] H. Xu, J. Zhang, J. Cai, H. Rezaatofghi, and D. Tao, "Gmflow: Learning optical flow via global matching," in *IEEE Conf. Comput. Vis. Pattern Recognit. (CVPR)*, 2022, pp. 8121–8130.
- [15] C. Harris, M. Stephens *et al.*, "A combined corner and edge detector," in *Alvey vision conference*, vol. 15, no. 50, 1988, pp. 10–5244.
- [16] J. Shi *et al.*, "Good features to track," in *IEEE Conf. Comput. Vis. Pattern Recognit. (CVPR)*, 1994, pp. 593–600.
- [17] D. G. Lowe, "Distinctive image features from scale-invariant keypoints," *Int. J. Comput. Vis.*, vol. 60, pp. 91–110, 2004.
- [18] E. Rublee, V. Rabaud, K. Konolige, and G. Bradski, "ORB: An efficient alternative to SIFT or SURF," in *IEEE Int. Conf. Comput. Vis. (ICCV)*, 2011, pp. 2564–2571.
- [19] X. Zhang, F. X. Yu, S. Karaman, and S.-F. Chang, "Learning discriminative and transformation covariant local feature detectors," in *IEEE Conf. Comput. Vis. Pattern Recognit. (CVPR)*, 2017, pp. 6818–6826.
- [20] D. DeTone, T. Malisiewicz, and A. Rabinovich, "Superpoint: Self-supervised interest point detection and description," in *IEEE Conf. Comput. Vis. Pattern Recognit. (CVPR)*, 2018, pp. 224–236.
- [21] A. Barroso-Laguna, E. Riba, D. Ponsa, and K. Mikolajczyk, "Key. net: Keypoint detection by handcrafted and learned cnn filters," in *IEEE Int. Conf. Comput. Vis. (ICCV)*, 2019, pp. 5836–5844.
- [22] X. Zhao, X. Wu, J. Miao, W. Chen, P. C. Chen, and Z. Li, "Alike: Accurate and lightweight keypoint detection and descriptor extraction," *IEEE Trans. Multimed.*, 2022.
- [23] X. Glorot, A. Bordes, and Y. Bengio, "Deep sparse rectifier neural networks," in *Proceedings of the fourteenth international conference on artificial intelligence and statistics*, 2011, pp. 315–323.
- [24] H. Germain, V. Lepetit, and G. Bourmaud, "Neural Reprojection Error: Merging Feature Learning and Camera Pose Estimation," in *IEEE Conf. Comput. Vis. Pattern Recognit. (CVPR)*, 2021, pp. 414–423.
- [25] Z. Li and N. Snavely, "MegaDepth: Learning Single-View Depth Prediction From Internet Photos," in *IEEE Conf. Comput. Vis. Pattern Recognit. (CVPR)*, June 2018.
- [26] D. P. Kingma and J. Ba, "ADAM: A method for stochastic optimization," *preprint arXiv:1412.6980*, 2014.
- [27] M. Trajković and M. Hedley, "Fast corner detection," *Image and vision computing*, vol. 16, no. 2, pp. 75–87, 1998.
- [28] V. Balntas, K. Lenc, A. Vedaldi, and K. Mikolajczyk, "HPatches: A benchmark and evaluation of handcrafted and learned local descriptors," in *IEEE Conf. Comput. Vis. Pattern Recognit. (CVPR)*, 2017, pp. 5173–5182.
- [29] M. A. Fischler and R. C. Bolles, "Random sample consensus: a paradigm for model fitting with applications to image analysis and automated cartography," *Communications of the ACM*, vol. 24, no. 6, pp. 381–395, 1981.
- [30] D. Zuñiga-Noël, A. Jaenal, R. Gomez-Ojeda, and J. Gonzalez-Jimenez, "The UMA-VI dataset: Visual-inertial odometry in low-textured and dynamic illumination environments," *Int. J. Rob. Res.*, vol. 39, no. 9, pp. 1052–1060, 2020.
- [31] M. Burri, J. Nikolic, P. Gohl, T. Schneider, J. Rehder, S. Omari, M. W. Achtelik, and R. Siegwart, "The EuRoC micro aerial vehicle datasets," *Int. J. Rob. Res.*, vol. 35, no. 10, pp. 1157–1163, 2016.
- [32] C. Campos, R. Elvira, J. J. G. Rodriguez, J. M. Montiel, and J. D. Tardós, "ORB-SLAM3: An accurate open-source library for visual, visual-inertial, and multimap slam," *IEEE Trans. Robotics*, vol. 37, no. 6, pp. 1874–1890, 2021.